

**Nanoscopic Analyses of Protein Adsorption on Poly(2-methoxyethyl acrylate) Surfaces for Tailoring Cell Adhesiveness**

Journal:	<i>Biomaterials Science</i>
Manuscript ID	BM-ART-01-2022-000093.R2
Article Type:	Paper
Date Submitted by the Author:	25-Mar-2022
Complete List of Authors:	Nishida, Kei; Kyushu University, Institute for Materials Chemistry and Engineering Baba, Koki; Kyushu University, Graduate School of Engineering Murakami, Daiki; Kyushu University, Institute for Materials Chemistry and Engineering; Kyushu University, Graduate School of Engineering Tanaka, Masaru; Kyushu University, Institute for Materials Chemistry and Engineering; Kyushu University, Graduate School of Engineering

ARTICLE

Nanoscope Analyses of Cell-Adhesive Proteins Adsorption on Poly(2-methoxyethyl acrylate) Surfaces

Kei Nishida,^a Koki Baba,^b Daiki Murakami,^{*a,b} and Masaru Tanaka,^{*a,b}

Received 00th January 20xx,
Accepted 00th January 20xx

DOI: 10.1039/x0xx00000x

Regulation of protein adsorption on the surface of biomaterials is important for modulating cell adhesion. Two important proteins in this regard are fibrinogen and fibronectin. Poly(2-methoxyethyl acrylate) (PMEA) and its derivatives have been developed as promising coating materials for biomaterial surfaces. Previous studies have highlighted that PMEA-coated substrates suppress thrombogenicity but promote cell adhesiveness. However, it was unclear what was responsible for these differences in adhesion. In this study, we focused on the correlation between protein adsorption and the nanometer-scale structures on the surfaces of the PMEA substrates. Atomic force microscopy using protein- or antibody-conjugated cantilevers were used to perform nanoscopic analyses of the adsorption forces and conformational changes in fibrinogen and fibronectin adsorbed on the nanometer-scale PMEA structures. The adsorption force of fibronectin in the polymer-poor regions was higher than that of fibrinogen, whereas the polymer-rich region showed a negligible difference in adsorption force between the two proteins. Interestingly, a greater conformational change in the adsorbed fibronectin was induced in the polymer-poor region than that of fibronectin in the polymer-rich region or that of fibrinogen in either region, resulting in the induction of cell adhesion. Nanoscopic analyses of protein adsorption on biomaterial surfaces promise insights for the design of novel biomaterials to control protein adsorption and cell adhesion.

Introduction

Biomaterial design has greatly contributed to the development of medical and therapeutic devices such as artificial blood vessels, orthopedic implants, dental materials, and extracorporeal membrane oxygenation systems.^{1–4} Polymeric biomaterials have been widely investigated owing to their ease of fabrication and functionalization.⁵ For example, commercial artificial blood vessels are mostly made of polyethylene terephthalate, polyurethane, or polytetrafluoroethylene. In addition, polymer coating is an effective approach to functionalizing biomaterial surfaces. Functionalization with poly(ethylene glycol) and zwitterionic polymers, including poly(2-methacryloyloxyethyl phosphorylcholine) (PMPC), suppresses biofilm formation,

immune responses to the biomaterial surfaces, and the adhesion of platelets and bacteria.^{6–9}

Poly(2-methoxyethyl acrylate) (PMEA) is an advanced polymeric material used as a biomaterial coating.^{10,11} PMEA coatings, which display antithrombogenicity, have been used in artificial heart–lung bypass systems and to coat metallic stents. When considering the biological reaction on biomaterials with bodily fluids, including blood, the first step is to be the protein adsorption on the materials.¹² Previously, we revealed that the hydration state of PMEA affected the amount of adsorption and the conformational changes in the proteins.¹³ From differential scanning calorimetry (DSC) measurements, three types of hydration states, non-freezing water (NFW), intermediate water (IW), and free water (FW), were observed in hydrated PMEA. Furthermore, the IW content of PMEA could be regulated by the systematic synthesis of PMEA derivatives, which indicates that the IW content in the polymers is an important factor for the protein adsorption behavior. An increase in IW content of the PMEA derivatives suppressed the adsorption and conformational changes in fibrinogen, which are related to the process of thrombogenicity with the adhesion and activation of platelet.^{14,15}

Conversely, PMEA promoted cell adhesion and regulated cell functions such as proliferation and differentiation.^{16–18} In addition, the droplets formed from PMEA selectively accumulated to tumor cells rather than to normal cells.¹⁹ This is because the PMEA-coated surface enhanced the conformational changes in adsorbed fibronectin, an adhesive cell protein.^{20,21} The adsorption behaviors of fibrinogen and

^a Institute for Materials Chemistry and Engineering, Kyushu University, 744 Motoooka, Nishi-ku Fukuoka 819-0395, Japan.

^b Graduate School of Engineering, Kyushu University, 744 Motoooka, Nishi-ku Fukuoka 819-0395, Japan.

† Corresponding Authors

* daiki_murakami@ms.ifoc.kyushu-u.ac.jp (D.M)

* masaru_tanaka@ms.ifoc.kyushu-u.ac.jp (M. T)

ORCID

Kei Nishida (K.N.): 0000-0001-6493-5436

Daiki Murakami (D.M.): 0000-0002-5552-4384

Masaru Tanaka (M.T.): 0000-0002-1115-2080

Present Addresses

Kei Nishida - Department of Life Science and Technology, School of Life Science and Technology, Tokyo Institute of Technology, Japan.

Electronic Supplementary Information (ESI) available: [details of any supplementary information available should be included here]. See DOI: 10.1039/x0xx00000x

fibronectin on PMEA-coated surfaces are different, which causes the unique property of PMEA that it displays both antithrombogenicity and cell adhesiveness. However, given the surface properties of PMEA, the origin of such a large difference in the behavior of fibrinogen and fibronectin is unclear. In this regard, using atomic force microscopy (AFM), we discovered that the PMEA-coated surface formed nanometer-scale protrusions on which PMEA spontaneously assembles.^{22–24} This is attributed to the phase separation of the polymer and water, and the nanometer-scale structures are classified as polymer-rich regions (the protrusions) and polymer-poor regions (the flat areas). The regions could affect the interaction of proteins with PMEA-coated surface due to the polymer density which altered the hydrophobicity and water content of the regions. We hypothesized that a nanoscopic and quantitative analysis of both fibrinogen and fibronectin adsorption on PMEA clarified the antithrombogenicity and cell adhesiveness of PMEA.

Herein, we establish methodologies for nanoscopic and quantitative analyses of protein adsorption using AFM and investigate the adsorption behavior of fibrinogen and fibronectin on PMEA-coated surfaces. First, the distribution of adsorbed proteins on the nanometer-scale structures of PMEA was estimated from the change in the elastic modulus of the PMEA/water interface where the proteins were adsorbed. Second, the adsorption forces of the proteins on the nanometer-scale structures of PMEA were analyzed using force measurements. Fibrinogen- and fibronectin-conjugated cantilevers were fabricated for this purpose. Finally, the conformational changes in the proteins adsorbed on the nanometer-scale structures of PMEA were estimated. These measurements used AFM with cantilevers conjugated with monoclonal antibodies that recognize specific domains of fibrinogen and fibronectin. These experiments revealed that fibrinogen tended to adsorb in the polymer-rich region, whereas fibronectin adsorbed in both the polymer-rich and polymer-poor regions of the PMEA substrate. Interestingly, the conformational change in the adsorbed fibronectin was enhanced in the polymer-poor region of the PMEA substrate in comparison with that of fibrinogen. The adsorption behaviors of fibrinogen and fibronectin on PMEA are affected by the hydrophilicity and water content of the nanometer-scale structures. These nanoscopic analyses of protein adsorption on PMEA substrates provide insight into the potential design of biomaterials that control antithrombogenicity and cell adhesiveness.

Experimental

Reagents

PMEA was synthesized according to previously reported methods (Figure S1, Table S1).^{11,15,17} Poly(2-methacryloyloxyethyl phosphorylcholine-*co-n*-butyl methacrylate) (30 : 70mol%) (PMPC; Lipidure-CM5206) was obtained from NOF CORPORATION (Tokyo, Japan). 3-Aminopropyltriethoxysilane, carboxy acid-poly(ethylene glycol)-*N*-hydroxysuccinimide ester (HOOC-PEG₁₃-NHS ester) ($M_n =$

787, extended chain length: 4.5 nm), *N*-hydroxy succinimide, fibrinogen (from human plasma), fibronectin (from human plasma) were purchased from Sigma-Aldrich. 1-Ethyl-3-(3-dimethylaminopropyl)carbodiimide was from Wako, trimethoxy(propyl)silane was from Tokyo Chemical Ind. 2,2'-Azinobis(3-ethylbenzothiazoline-6-sulfonic acid ammonium salt) (ABTS) was from Roche Life Science, and Blocking One was from Nacalai tesque. Other reagents and solvents were obtained from Kanto Chemical (Tokyo, Japan).

Instruments

The contact angle values of PMEA analogues surfaces were calculated from the sessile drop of water at 25°C using a DropMaster DMO-501SA goniometer (Kyowa Interface Science Co., Tokyo, Japan). Scanning electron microscopic images were acquired by a Keyence VE-9800 scanning electron microscope. X-ray Photoelectron Spectroscopic (XPS) spectra were recorded by APEX ESCA instrument (ULVAC-PHI, Kanagawa, Japan).

Fabrication and characterization of PMEA-coated substrates

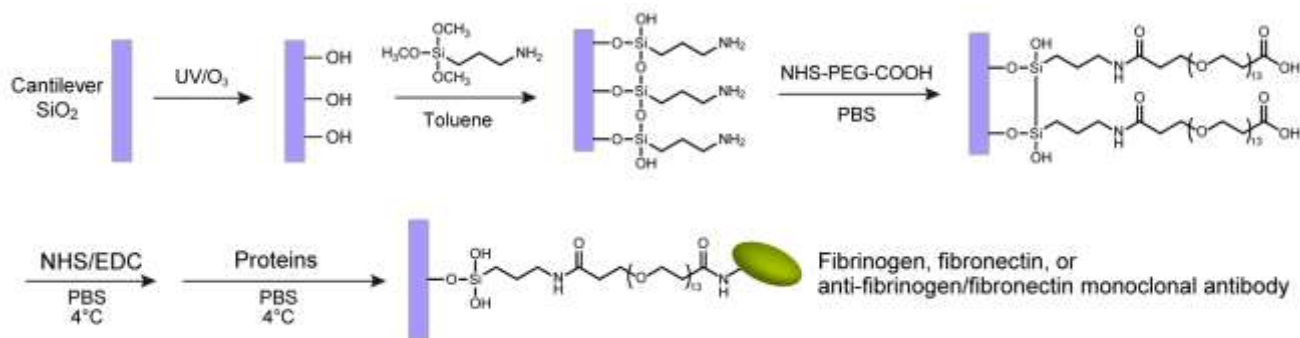
Polyethylene terephthalate (PET) sheet (thickness = 120 μm) (Mitsubishi Chemical, Tokyo, Japan) was cut out into a circle with a diameter of 14 mm. PMEA solution (0.2 wt%) dissolved in methanol were spin-coated on the PET substrates using a Mikasa Spin Coater MS-A100 at the consecutive rates of 500 rpm for 5 s, 2000 rpm for 10 s, a ramp up for 5 s, 4000 rpm for 5 s, and a ramp down for 4 s and was then dried.

AFM observation

AFM was carried out by Bioscope Resolve (Bruker, Billerica, MA, USA) with peak force tapping mode. SNL-10-B cantilever (spring constant: 0.12 N m⁻¹, tip radius < 12 nm, Bruker) was used as is for topographic imaging of the polymer/PBS interfaces. The feedback setpoint was set to 1.0 nN. The topographic and elastic imaging of the interfaces after protein adsorption was performed with SNL-10-A cantilever (spring constant: 0.35 Nm⁻¹, tip radius < 12 nm, Bruker) and the feedback setpoint of 3.0 nN. 10 μg mL⁻¹ protein/PBS solutions were put on the PMEA surface, and the interfacial images at 0, 10, 30, and 60 min. after the deposition were obtained in the solutions. The feedback setpoint was set to 3.0 nN. For both cases, the scan rate was 5.0 μm s⁻¹ and the investigations were carried out at room temperature.

Enzyme-linked immuno-sorbent assay (ELISA)

PMEA substrate was incubated with PBS for 1 h at 37 °C. After removing the supernatant, PMEA substrate was immersed in solutions of fibrinogen (10 μg mL⁻¹) and fibronectin (10 μg mL⁻¹) dissolved in PBS at 37 °C for 10 min. Blocking One was treated with the substrate for 60 min at room temperature. Then, mouse anti-human fibrinogen γ-chain antibody (clone 2.G2.H9; Santa Cruz Biotechnology Inc) (1:1000) and mouse anti-human fibronectin RGD-sequence antibody (Clone FN-12-8, Takara clontech.) (1:1000) at room temperature for 90 min, and subsequently treated with



Scheme 1. Fabrication of protein-conjugated cantilever

HRP-conjugated goat anti-mouse IgG (H+L) antibody (1:5000 dilution) at 37°C for 2 h. After washing by PBS twice, ABTS (1 mg mL⁻¹) solution was treated with the substrate at 37°C for 30 min. The absorbance was measured at a wavelength of 405 nm using Infinite 200PRO M Plex microplate reader (Tecan, Zürich, Switzerland).

Modification of cantilever (Scheme 1)

The SNL-10-B and MSNL-10-A (spring constant: 0.07 Nm⁻¹, tip radius < 12 nm, Bruker) cantilevers were used for the modification with proteins and antibody, respectively. The cantilevers were washed with water and ethanol, and subsequently irradiated with UV/O₃ for 30 min using UV ozone cleaner (Filgen Inc., UV253E(R)) twice. (3-Aminopropyl)triethoxysilane dissolved in toluene (1 v/v%) was treated with cantilevers for 1 h. After washing with toluene, reacted cantilevers were dried at 100°C for 1 h under vacuum. The obtained cantilevers were immersed with the solution of HOOC-PEG₁₃-NHS ester (1 mg mL⁻¹) dissolved in PBS for 1 h. The reacted cantilevers were treated with 1-ethyl-3-(3-dimethylaminopropyl)carbodiimide (0.1 M) and *N*-hydroxy succinimide (0.1 M) dissolved in PBS at 4°C for 1 h. After washing with PBS, the solution of fibrinogen (10 µg mL⁻¹) and fibronectin (10 µg mL⁻¹) were treated with the cantilevers at 4°C for 1 h. The reacted cantilevers were washed with PBS twice to obtain fibrinogen- and fibronectin-conjugated cantilevers. Proteins-conjugated silicon wafer was synthesized in the same manner. Additionally, antibodies-conjugated cantilevers were synthesized in the same manner using mouse anti-human fibrinogen γ -chain antibody and mouse anti-human fibronectin RGD-sequence antibody.

For the fabrication of hydrophobized cantilevers, UV/O₃-irradiated cantilevers (SNL-10-B) were reacted with trimethoxy(propyl)silane dissolved in toluene (1 v/v%) for 1 h. After washing with toluene, the reacted cantilevers were dried at 100°C under vacuum to obtain the hydrophobized cantilevers. Hydrophobized silicon wafer was synthesized in the same manner.

Force measurement

The force measurements with the protein-conjugated cantilevers were performed on PMPC, PET and PMEA in PBS. In the case of PMEA, the measured points were classified into polymer-rich or polymer-poor regions from their height variation. The measurements were done at 50 points for each PMPC, PET, PMEA

polymer-rich and PMEA polymer-poor with the forwarding and retracting velocities of 1.0 µm s⁻¹ and the setpoint of 1.0 nN. The adsorption force and the adsorption energy (the integration of force-distance curve) were obtained from the retraction curves. The force measurements with the hydrophobized cantilevers were performed in the same manner.

For the force measurements with the antibody-conjugated cantilevers, first the 10 µg mL⁻¹ protein/PBS solutions were deposited on the polymer samples for 10 min. and rinsed with PBS 3 times. Then the interaction between the protein adsorbed polymer surfaces and the antibodies were measured (the forwarding and retracting velocities were 20 µm s⁻¹ and the setpoint was 2.0 nN). The results obtained at 50 points for each combination of fibrinogen, fibronectin and polymer-rich, polymer-poor regions were used for analysis.

Statistical analysis

Data are means \pm SD of at least three independent trials. Significant differences between treatment means were assessed by one-way ANOVA followed by the Tukey-Kramer multiple comparison test in OriginPro v. 2020b (OriginLab, Northampton, MA, USA). Statistical significance was set at $P < 0.05$.

Results and discussion

Macroscopic analyses of protein adsorption on PMEA substrates

For cell adhesion, it is important that the binding site of the adsorbed protein is exposed on the biomaterial surface.^{25–27} The relevant binding sites in this study are the γ -chain of fibrinogen is related to the adhesion and activation of platelets, leading to thrombogenesis. The arginine–glycine–aspartic acid (RGD) sequence of fibronectin is related to the adhesion of adherent cells such as fibroblasts, endothelial cells tumor cells, and stem cells.^{28,29} We first evaluated the amount of fibrinogen and fibronectin, with exposed binding sites, adsorbed onto a PMEA substrate (**Figure 1a,b**). The PMEA substrates were fabricated by spin-coating of the PMEA onto a PET substrate. In our previous research, transmission

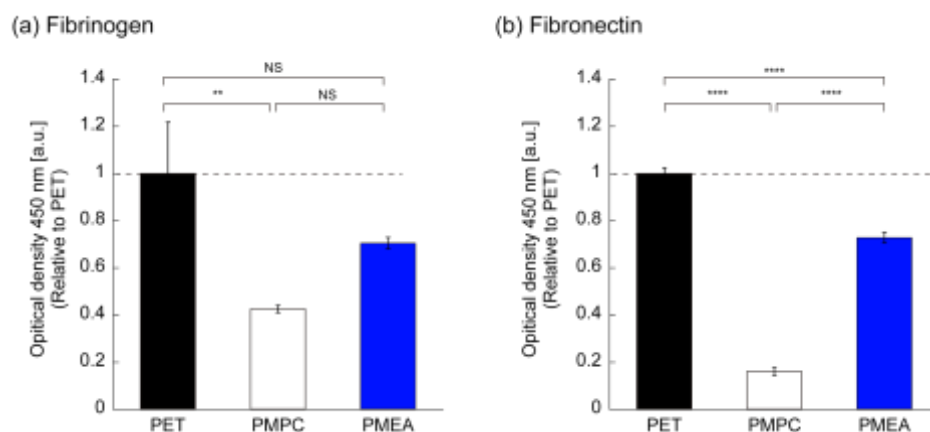


Figure 1 (a,b) The amount of γ -chain of adsorbed fibrinogen (a) and RGD-sequence of adsorbed fibronectin (b) on the surfaces analyzed by indirect ELISA. Data were expressed as mean \pm SD ($n = 3$, ** $p < 0.01$, **** $p < 0.0001$, NS: not significant).

electron microscopy observation revealed that the thickness of the PME A layer fabricated by spin-coating was approximately 70–80 nm³⁰. A PMPC-coated PET substrate was also prepared as a negative control for protein adsorption. The PET, PMPC, and PME A substrates were exposed to fibrinogen or fibronectin for 10 min and subsequently characterized by indirect ELISA. The optical values from the ELISA results, which are related to the amount of exposure of the binding groups, were expressed relative to those of PET. The exposures of the γ -chains (fibrinogen) and RGD-sequences (fibronectin) on the PME A and PMPC substrates were lower than those on PET. From micro BCA assay, the quantity of adsorbed proteins on the substrate surfaces after 10 min of adsorption, showed large errors (**Figure S2**). Our previous reports demonstrated that PME A tended to suppress the adsorptions and conformational changes of serum proteins on its surface^{13–15}. Although the quantities of adsorbed proteins on the substrate surfaces after 10 min of adsorption time were unclear, it suggests that the PME A substrates suppressed conformational changes in the adsorbed fibrinogen and fibronectin.

Nanoscope analyses of protein adsorption on PME A substrate

From AFM, the surface of PME A in phosphate-buffered saline (PBS) showed the formation of protrusions in the surface structure, which were polymer-rich, and flat regions, which were polymer-poor, in agreement with our previous reports.²² In contrast, the surface of PET and PMPC-coated PET at the water interface were smooth (**Figure 2**). To investigate the

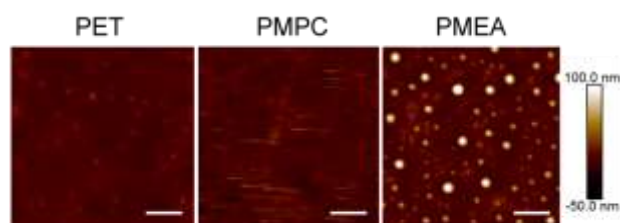


Figure 2. Topographic images of surface on PET coated with PMPC and PME A acquired by AFM in PBS (Scale bars: 1 μ m).

relationship between the nanostructure of the PME A substrate and the protein adsorption, the distributions of fibrinogen and fibronectin adsorbed on the PME A substrates were measured by the changes in the height and elastic modulus of the substrate with adsorbed proteins. From the height images, no significant differences in the adsorption of fibrinogen and fibronectin on the PME A substrates are noted (**Figure 3a,b**). Our previous reports demonstrated that the amounts of fibrinogen and fibronectin adsorbed onto the PME A substrates were consistent with their monolayer configurations, resulting in negligible changes in their heights^{14,31}. In contrast, these substrates exhibited a decrease in the elastic modulus of the surface in a time-dependent manner. The histograms for the elastic moduli of the protein-adsorbed substrates were constructed from their moduli images (Figure 3a,b). Considered alongside the height images, we confirmed that the elastic modulus of the polymer-poor region corresponded to $\log(\text{Pa}) > 8.0$, and that of the polymer-rich region to $\log(\text{Pa}) < 7.5$. In the polymer-poor regions of the PME A, the fibronectin treatment significantly decreased the elastic modulus in a time-dependent manner in comparison with fibrinogen, resulting that fibronectin might adsorb onto the polymer-poor regions. In contrast, the elastic modulus of the polymer-rich region showed a slight change after the adsorption of both proteins. Although fibronectin might adsorb onto the polymer-poor region of PME A, the detailed adsorption behavior was still unclear from these measurements.

Adsorption force of proteins on the nanometer-scale structures of PME A

Next, we evaluated the adsorption force of fibrinogen and fibronectin on the PME A substrate to estimate the distribution of adsorbed fibrinogen and fibronectin in polymer-poor or rich regions of the PME A substrates. This was done by AFM using fibrinogen- and fibronectin-conjugated cantilevers. The surfaces of the silicon nitride cantilevers were modified with carboxy group-terminated poly(ethylene glycol) (repeat units:

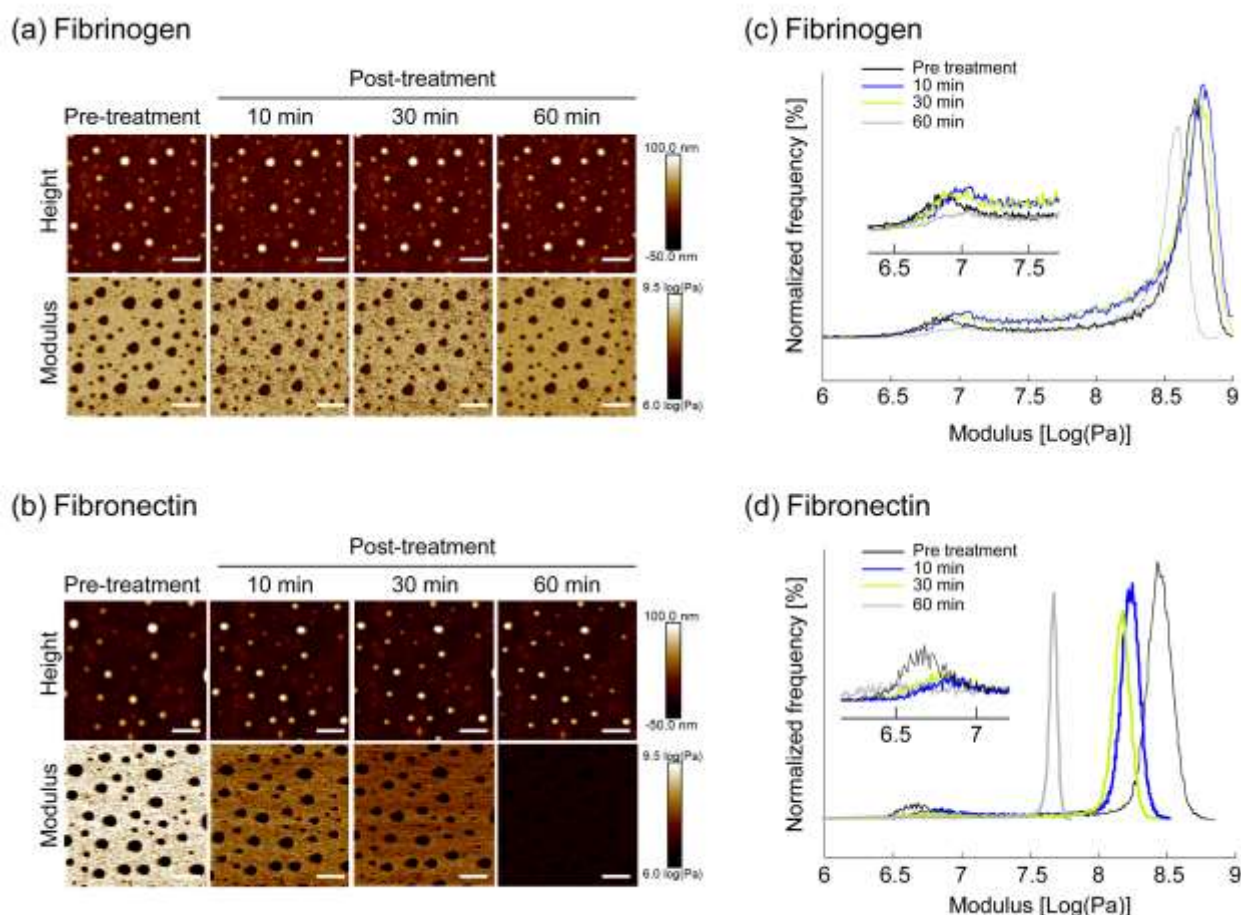


Figure 3 (a) Changes in height and log(modulus) images of PMEA surface treated with fibrinogen and (c) fibronectin for 10, 30, 60 min. (Scale bars: 1 μm). (b) Graph of the modulus of the PMEA substrates treated with fibrinogen and (d) fibronectin for 10, 30, 60 min.

13) (PEG₁₃-COOH) linkers, and these reacted with amine groups from the proteins via a condensation reaction (Scheme 1). However, it was difficult to confirm the conjugation of the protein on the triangular cantilever using X-ray photoelectron spectroscopy (XPS) because the sample size was too small. As an alternative, we confirmed the success of the reactions by measuring the protein conjugation to silicon wafers. XPS of these wafers showed that the elemental and chemical compositions of these surfaces showed a decrease in the ratios of Si and O, and an increase in the ratios of C and N after the modification with 3-aminopropyltriethoxysilane, PEG₁₃-COOH, and fibronectin (Figure 4a,b). Conjugated fibronectins on the silicon surface were also detected by ELISA and scanning electron microscopic images (Figure S3a,b). The protein-conjugated cantilevers exhibited lower elastic moduli on PET substrate compared to the unmodified cantilever (Figure S4). In addition, the elastic modulus of fibronectin was lower than that of fibrinogen. It suggests that the change in the elastic moduli of fibrinogen-adsorbed PMEA substrates was related to not only the less adsorption amount of fibrinogen but also the fact that its elastic modulus was equivalent to that of PMEA substrates (Figure 3c,d).

To measure the adsorption force of proteins on the PMEA surfaces, the PMEA surfaces were analyzed by AFM using the protein-conjugated cantilevers (Figure 4c). On PMPC substrates, the adsorption force of fibrinogen and fibronectin was lower than other polymer surfaces (Figure 4d). The adsorption force of fibronectin to PET substrates was higher than that of fibrinogen. On the PMEA surfaces, the adsorption force of fibronectin was significantly higher than that of fibrinogen in the polymer-poor regions, whereas there was no difference in the adsorption force of the proteins in the polymer-rich regions. The adsorption force of the protein-modified cantilevers to PMEA substrates increased with inducing the conformational change to the protein by urea treatment (Figure S5). In addition, there was little difference in the adsorption forces after repeated measurements using the protein-modified cantilevers (Figure S6). These results suggest that the conformational changes in the proteins that had conjugated on the cantilevers after the repeated measurements, were negligible. These results suggest that fibronectin tended to adsorb more strongly on the polymer-poor regions than fibrinogen, whereas both proteins adsorb equally well in the polymer-rich region.

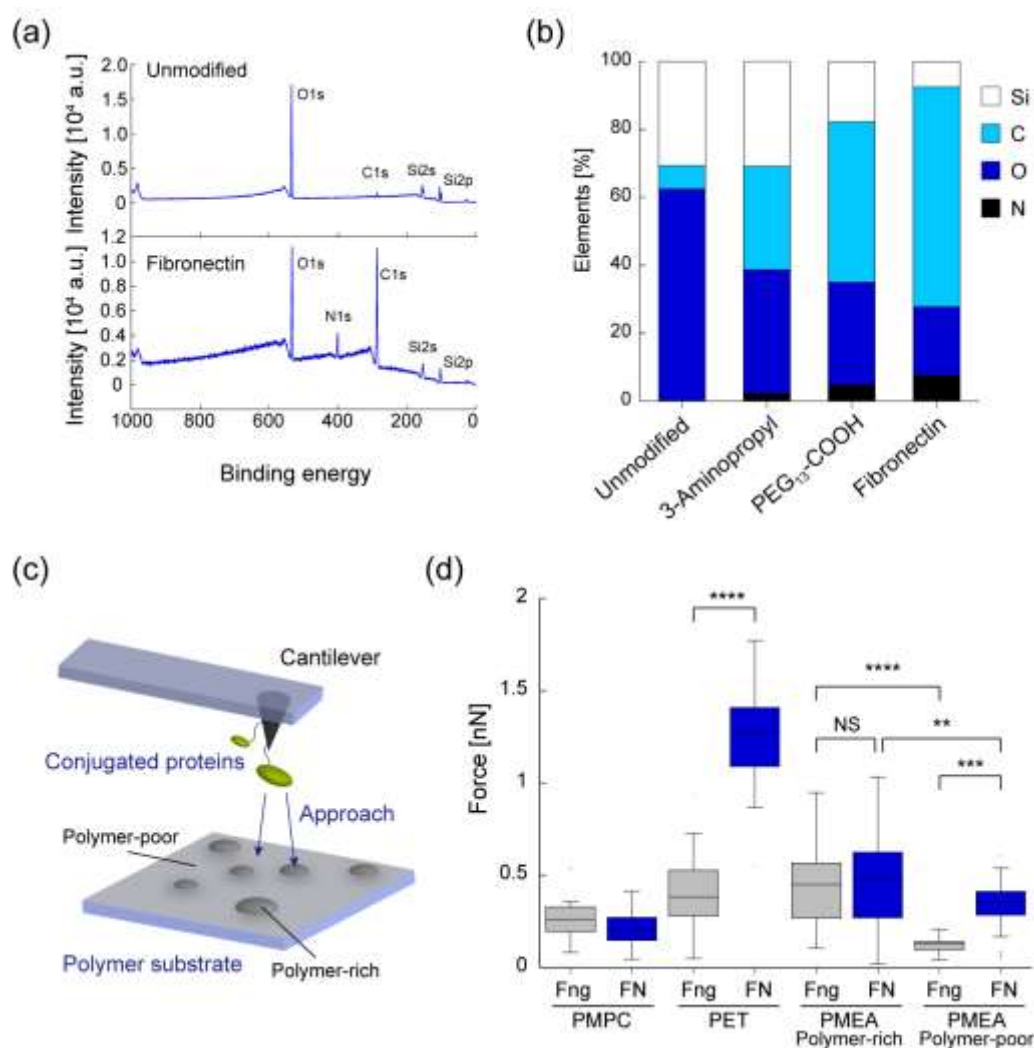


Figure 4 (a) XPS profiles of unmodified and fibronectin-conjugated silicon wafers. (b) XPS atomic ratios of different elements on unmodified, 3-aminopropyl, PEG₁₃-COOH-modified, and fibronectin-conjugated silicon wafers. (c) Schematic illustration for the measurement of the interaction of the protein-conjugated cantilever with polymer-rich or polymer-poor portion of the PMEAs substrate. (d) Box plots for the adhesion force of fibrinogen- (Fng) and fibronectin- (FN) conjugated cantilevers interacting with PMPC, PET and the polymer rich and poor regions of PMEAs. Data were expressed as mean \pm SD ($n = 50$, *** $p < 0.001$, **** $p < 0.0001$, NS: not significant).

Considering that PMEAs are water-insoluble (hydrophobic) polymers, hydrophobic interactions between proteins and PMEAs should dominate. The hydrophobicity of the PMEAs substrate differs between polymer-rich and polymer-poor regions. It suggests that the difference in the adsorption behavior between fibrinogen and fibronectin depends on the properties of the surface such as hydrophobic/hydrophilic balance. When protein adsorption occurs on surfaces of biomaterials, the conformational changes proceed in a time-dependent manner, and lead to the exposure of hydrophobic segments in the proteins.^{32,33} Molino et al. used a quartz crystal microbalance with dissipation monitoring to demonstrate that the dynamic process of proteins adsorbing onto the substrate surface occurred over the duration of an hour or longer³⁴. An increase in the contact time of the proteins would increase their adsorption forces via the

conformational changes in the proteins. In addition, the adsorption forces of the proteins on the PMEAs substrate may be related to the ease of conformational change in the protein when in contact with the substrate.

Hydrophobicity of the nanometer-scale structures of PMEAs

The hydrophobicity of biomaterials plays a key role in regulating protein adsorption behavior on its surface.^{35,36} Because different regions of the PMEAs substrate have different polymer densities, these regions exhibit different hydrophobicities. It has been reported that the hydrophobicity measured by the contact angle method is related to the adsorption force of cantilevers measured by AFM.³⁷ Hydrophobized cantilevers were therefore used to acquire force curves in order to measure the hydrophobicities of the various regions of the PMEAs surfaces through the strength of

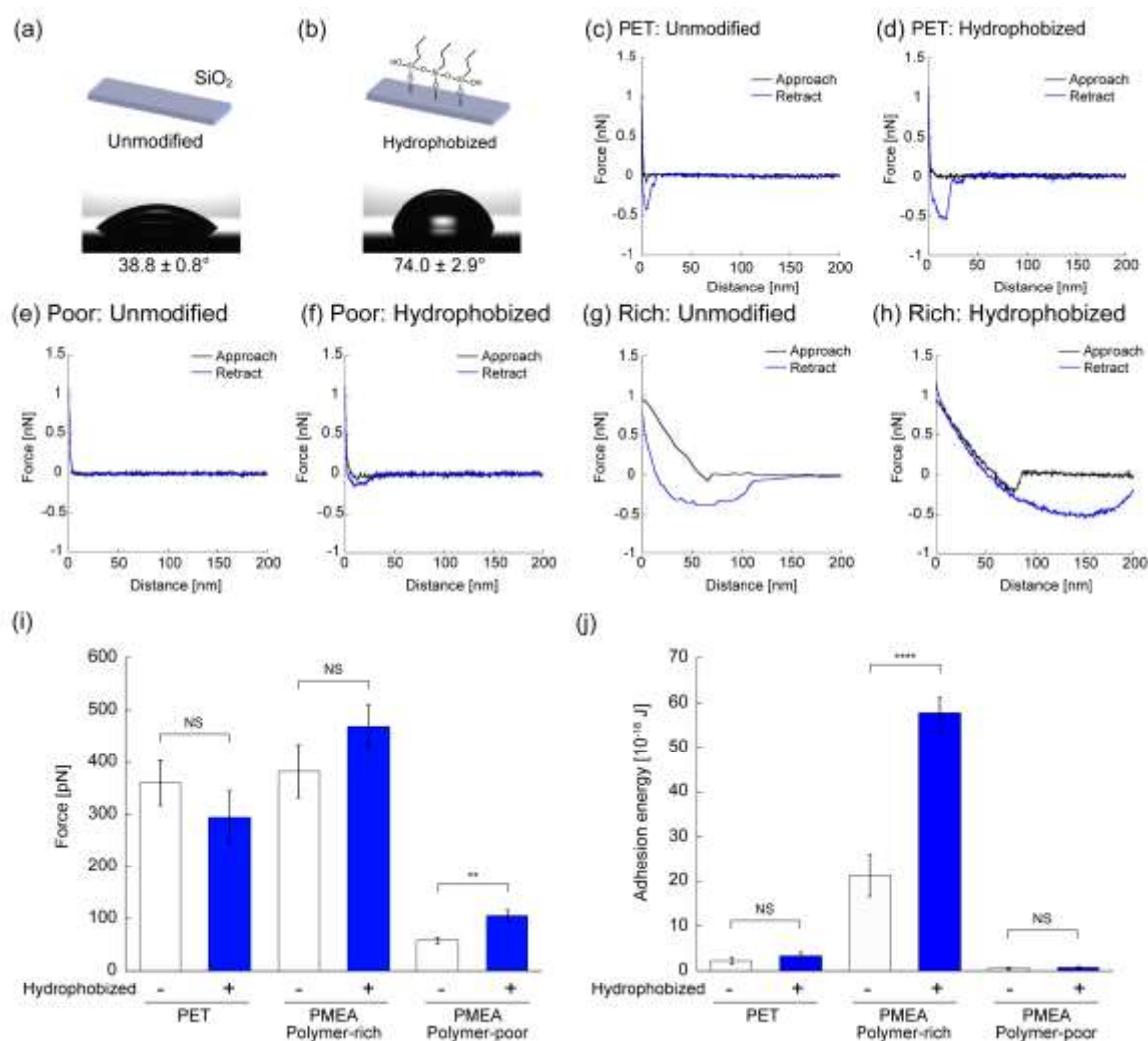


Figure 5 (a,b) Contact angle images for droplets of water on unmodified (a) and hydrophobized (b) silicon wafer as model surface of cantilever. (c-h) Representative force curves for unmodified and hydrophobized cantilevers in contact with: (c, d) the PET substrate, (e, f) the polymer-poor region of PMEA, and (g, h) the polymer-rich region of PMEA. (i, j) (i) Adhesion force and (j) energy of the unmodified and hydrophobized cantilevers in contact with the PET substrate, the polymer-rich and polymer-poor regions of PMEA. Data were expressed as mean \pm SD ($n = 50$, *** $p < 0.001$, **** $p < 0.0001$, NS: not significant).

the hydrophobic interactions in PBS. The silicon nitride cantilever was modified using trimethoxy(propyl)silane, a silane coupling reagent. A silicon wafer was again used as a proxy for the cantilever to measure the modification of cantilever. Trimethoxy(propyl)silane-modified silicon wafer showed an increase in the contact angle compared to the unmodified silicon wafer, suggesting that the cantilever was hydrophobized (Figure 5a,b).

From the retraction curves, the PET surface and both regions of the PMEA surface experienced an attractive force towards both the unmodified and the hydrophobized cantilevers (Figure 5c-h). The adsorption force of both cantilevers to the polymer-poor regions was lower than that of polymer-rich regions, indicating that the polymer-rich regions of PMEA were more hydrophobic than the polymer-poor regions (Figure 5i). The adsorption energy was higher for

the polymer-rich regions compared to the other surfaces owing to the entanglement of polymer chains (Figure 5j). Moreover, the hydrophobized-cantilever in contact with the polymer-rich regions showed a three-fold higher value of adsorption energy in comparison with the unmodified cantilever. This also suggests that the polymer-rich regions of PMEA had a higher affinity for hydrophobic molecules than the polymer-poor regions. Our previous reports have mentioned that polymer-poor regions of the PMEA substrate would be water-rich.^{22,38} Therefore, the polymer-poor regions of PMEA showed higher hydrophilicity than the polymer-rich regions, which leads to differences in the distribution and adsorption force of the proteins in these regions. It has been reported that fibronectin adsorbed on biomaterial surfaces exhibits a more favorable conformation in hydrophilic regions compared to hydrophobic regions, whereas the conformational changes in

fibrinogen were increased in hydrophobic regions.³⁹ The distributions and adsorption forces of fibrinogen and fibronectin on the nanoscale structures of PMEAs help to determine their conformational changes.

Conformational changes in adsorbed proteins in relation to the nanometer-scale structures of PMEAs

Finally, the conformational changes in adsorbed fibrinogen and fibronectin in relation to the nanometer-scale structures

of PMEAs were investigated. We have developed a method to quantitatively measure the conformational change in adsorbed proteins on PMEAs by AFM. The cantilever and silicon wafer substrates were modified with monoclonal antibodies that recognize a cell-binding site of fibrinogen (γ -chain; Fib-cantilever) or fibronectin (RGD-sequence; FN-cantilever) via a PEG linker. The Fib-cantilever showed a significant attractive force of over 30 nm on fibrinogen-modified substrates (Figure 6a-c). Because the chain length of the PEG linker was

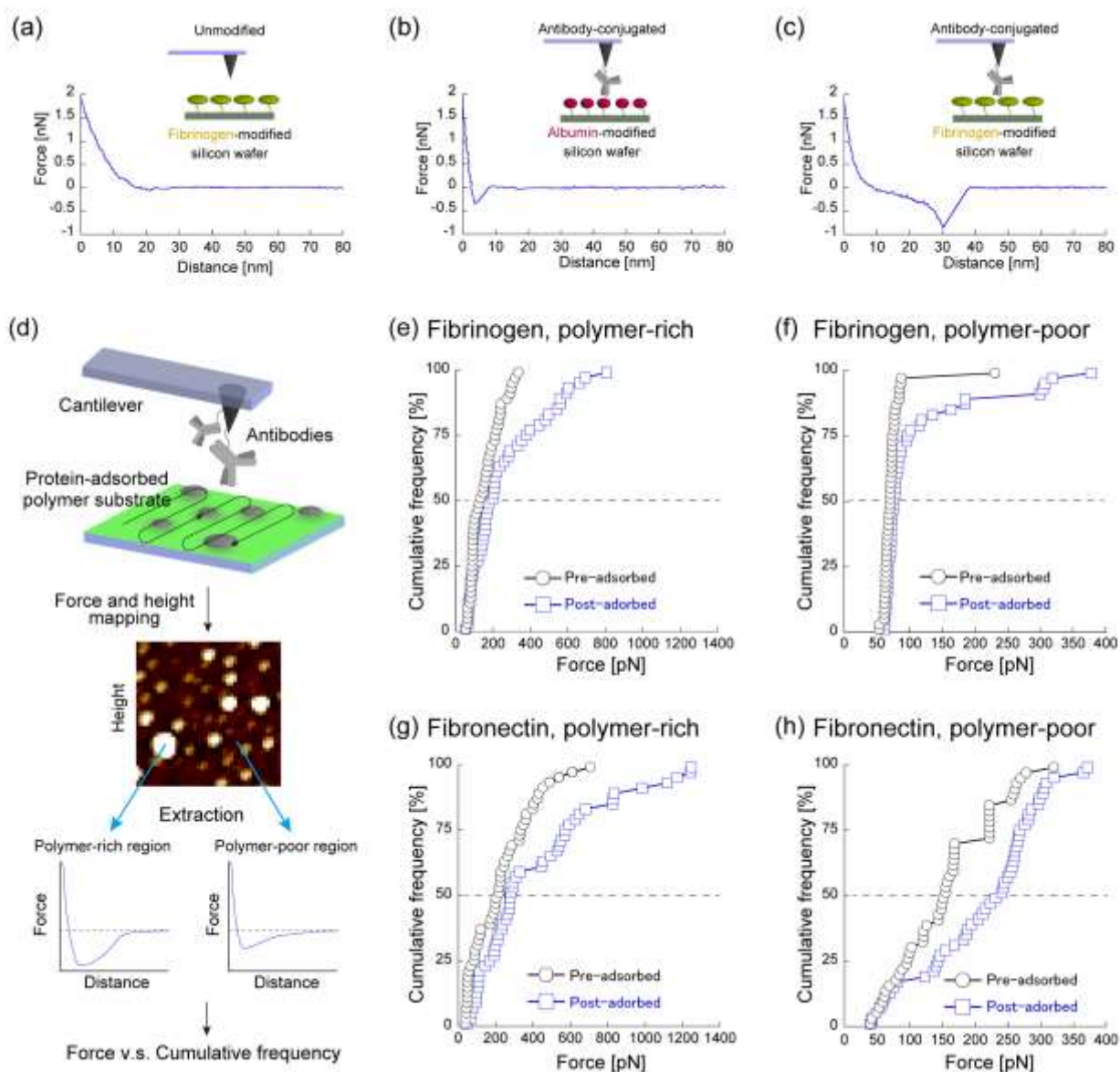


Figure 6. (a-c) Retraction curves: (a) between the unmodified cantilever and the fibrinogen-modified silicon wafer, (b) between the anti-fibrinogen monoclonal antibody-conjugated cantilever (fib-cantilever) and an albumin-modified silicon wafer, and (c) between the fib-cantilever and fibrinogen-modified silicon wafer. (d) Schematic illustration for the acquisition of the cumulative frequency plots of adhesion force, for measuring the interaction between the monoclonal antibody-conjugated cantilever and the protein-adsorbed PMEAs substrate. (e-h) Cumulative frequency plots of adhesion force; (e) between the fib-cantilever and the pre- or post-fibrinogen-adsorbed polymer-rich region, (f) the fib-cantilever and pre- or post-fibrinogen-adsorbed polymer-poor region, (g) between the anti-fibronectin monoclonal antibody-conjugated cantilever (FN-cantilever) and the pre- or post-fibronectin-adsorbed polymer-rich region, and (h) the FN-cantilever and pre- or post-fibronectin-adsorbed polymer-poor region. Data were expressed from 50 points of force curves.

Table 1 Summary of the relationship between the nanometer-scale structures of PMEA and proteins adsorption behavior

Region	Hydrophobicity	Adsorption force (nN)		Conformational change (%)	
		Fibrinogen	Fibronectin	Fibrinogen	Fibronectin
Polymer-rich	High	0.43 ± 0.18	0.45 ± 0.27	42	32
Polymer-poor	Low	0.12 ± 0.04	0.34 ± 0.13	24	76

estimated to be 4.5 nm, the force distance between the Fib-cantilever and the fibrinogen-modified substrate contained the length of the extended PEG-linker. In contrast, there were weak forces between the unmodified-cantilever and fibrinogen-modified substrate, or between the antibody-modified cantilever and an albumin-modified substrate. This confirms that the Fib-cantilever recognized the exposed γ -chain of adsorbed fibrinogen on the substrate. Therefore, the degree of the adsorbed proteins can be measured by the adsorption force between the antibody-modified cantilevers and the adsorbed proteins.

From the force and height maps acquired with the antibody-modified cantilevers on the protein-adsorbed PMEA substrates, we measured the force at 50 points each in the polymer-rich and polymer-poor regions. We then plotted the force and the cumulative frequency at which the force occurred (**Figure 6d**). Adsorbed fibrinogen and fibronectin with exposed binding sites increase the force applied to the antibody-modified cantilever compared to the substrate pre-protein adsorption, resulting in an increase in the incidence of large forces (**Figure 6e-h**). In the polymer-rich region, the differences in forces between the pre- and post-protein-adsorbed substrates increased significantly above 250 pN (**Figure 6e,g**). Fibrinogen adsorption on the PMEA surface increased the force on the Fib-cantilever by more than 100 pN, with a cumulative frequency of 68% (**Figure 6e**). Fibronectin adsorption in the polymer-rich region of PMEA increased the force applied to the FN-cantilever more than 250 pN with a cumulative frequency of 58% (**Figure 6g**). The antibodies modified on cantilevers recognize the exposed binding sites of the proteins on the substrates, resulting in an increase in antibody-protein interactions. The threshold for an antibody-protein interaction was set to 250 pN in the polymer-rich region, and suggests that 32% of the fibrinogen and 42% of the fibronectin adsorbed in the polymer-rich regions had exposed binding sites. On the other hand, the threshold for an antibody-protein interaction was set to 100 pN in the polymer-poor region because the force between the polymers and antibodies was small. The differences in force between pre- and post-protein-adsorbed substrates increased significantly above 100 pN in the polymer-poor region (**Figure 6f,h**). The threshold of this force was achieved in 76% of the fibrinogen-adsorbed polymer-poor region interactions, and in 24% of the fibronectin-adsorbed polymer-poor region interactions. These results suggest that 24% of the fibrinogen and 76% of the fibronectin adsorbed in the polymer-poor

regions that had exposed cell-binding sites. Therefore, the exposure of the RGD sequence of fibronectin was increased in the polymer-poor region, while the exposure of the γ -chain of fibrinogen was suppressed. Furthermore, we measured fibronectin-adsorbed PMPC substrates as control samples (**Figure S7**) because a significant difference between PMPC and PMEA was observed from the ELISA results regarding the conformational change in fibronectin (**Figure 1a**). The changes in the force values between pre- and post-protein-adsorbed PMPC substrates were negligible. Because the conformational change in fibronectin adsorbed onto PMPC was lower than that adsorbed onto PMEA, the results for the force-frequency measurements were consistent with the ELISA results. However, it is necessary to verify the generality of this measurement method using other polymer materials.

On the PMEA substrates, the degrees of the conformational changes in both adsorbed proteins in the polymer-rich region remain the same. Considering the adsorption force of fibrinogen and fibronectin (shown in **Figure 4**), the conformational changes in the proteins on the PMEA substrate were related to the adsorption force. Although the threshold values for the polymer-poor and polymer-rich regions were set to 250 pN and 100 pN, respectively, it was unclear whether the threshold values were suitable for measuring the conformational change in the adsorbed proteins. Further clarification is needed to investigate the relationship between the degree of conformational change of the adsorbed protein and the adsorption force of the antibody-conjugated cantilever.

It has been reported that the adhesion and activation of platelets is suppressed on PMEA-coated substrates, while the adhesion of cells is enhanced.^{11,15,16} In the present study, PMEA inhibited the conformational change in fibrinogen adsorbed on polymer-poor and rich regions, while adsorbed fibronectin showed greater conformational changes in the polymer-poor regions (**Table 1**). The nanometer-scale structures of the PMEA substrates play a key role in the adsorption and conformational change in the adsorbed proteins. Berglin et al. demonstrated that the conformational change in adsorbed fibrinogen on polymer surfaces was suppressed with decreasing glass transition temperature (T_g).⁴⁰ Because PMEA possessed a T_g of -49 °C in hydrated conditions, polymer chain flexibility could be one of the factors suppressing the conformational change in fibrinogen (**Table S1**). Our previous reports have demonstrated that the polymer-poor region (water-rich region) of PMEA might be

abundant in water, including non-freezing water (NFW) and intermediate water (IW), leading to the suppression of adsorption and conformational change in fibrinogen.⁴¹ Meanwhile, it has been reported that the conformational change in adsorbed fibronectin on a substrate was promoted more by hydrophilic surfaces compared to hydrophobic surfaces.^{34,42} In this regard, the hydrophilicity of the polymer-poor region was higher than that of the polymer-rich region (Figure 5). The hydrophilicity of the polymer-poor region of PMEA suppresses the exposure of the γ -chain of adsorbed fibrinogen, which is related to thrombogenicity, and enhances the exposure of the RGD-sequence of the adsorbed fibronectin, which is related to cell adhesiveness. The hydrophobic–hydrophilic balance at the water/PMEA interface is modulated by the formation of nanometer-scale structures, altering the adsorption and conformations of the adsorbed proteins. Consequently, protein adsorption behavior notably varies with the nanoscopic properties of surfaces; thus, nanoscopic evaluation is necessary for the design and characterization of biomaterial surfaces, including PMEA. In addition, further investigation is needed to reveal the effect that the conformations of proteins conjugated on cantilevers have on the results of the measurements, and the effect of the nanoscopic properties of the substrate surfaces on their protein adsorption behavior. These can be done using AFM-based infrared spectroscopy, scattering-type scanning near-field optical microscopy, and surface-assisted laser desorption/ionization mass spectrometry imaging.^{43–45}

Conclusions

This study detailed the nanoscopic analyses of protein adsorption on the nanoscale structures of PMEA substrates. The polymer-rich and -poor regions on PMEA substrates exhibited different protein adsorption behaviors, such as adsorption force and conformation changes. There was no significant difference in the adsorption behavior between fibrinogen and fibronectin in the polymer-rich region. Meanwhile, the polymer-poor region displayed increased adsorption force and enhanced conformational change in fibronectin in comparison with fibrinogen. This suggests that the hydrophilicity and water content of the polymer-poor region affected the interactions with fibrinogen and fibronectin. Hence, the conformations of fibrinogen and fibronectin adsorbed in the polymer-poor region would suppress the thrombogenicity and promote the cell adhesiveness, respectively. Taken together, nanoscopic analyses of biomaterials, including PMEA derivatives, play a key role in revealing detailed protein adsorption behavior, and can aid in the development of novel biomaterials that can regulate cell adhesion.

Author Contributions

Conceptualization of the research was conceived by D.M. and T.M. Design of the research was conceived by K.B. and K.N.. All

experiments and analyses were performed by K.B. and K.N.. The manuscript was written and edited by K.N., D.M. and M.T.. Reviewing the manuscript was performed by all authors. Funding acquisition was provided by D.M. and M.T.. This work was completed under supervision of M.T.

Conflicts of interest

There are no conflicts to declare.

Acknowledgements

This work was financially supported by following grants; (JSPS KAKENHI (grant number JP19H05720 to M.T. and 21K18066 to K.N.); the Funding Program for Next-Generation World-Leading Researchers (NEXT Program) of the Ministry of Education, Culture, Sports, Science and Technology (MEXT) of Japan and the Center of Innovation Program from the Japan Science and Technology Agency (JST). Additionally, this study was partially supported by the Dynamic Alliance for Open Innovation Bridging Human, Environment, and Materials.

Notes and references

Complete experimental methods and Figures S1, S2, S3, S4 and Table S1 were described in Supporting Information.

References

- 1 A. Ontaneda and G. M. Annich, *Front. Med.*, 2018, **5**, 1–9.
- 2 H. F. Guo, W. W. Dai, D. H. Qian, Z. X. Qin, Y. Lei, X. Y. Hou and C. Wen, *Acta Biomater.*, 2017, **54**, 107–116.
- 3 M. P. Staiger, A. M. Pietak, J. Huadmai and G. Dias, *Biomaterials*, 2006, **27**, 1728–1734.
- 4 K. L. Van Landuyt, T. Nawrot, B. Geebelen, J. De Munck, J. Snauwaert, K. Yoshihara, H. Scheers, L. Godderis, P. Hoet and B. Van Meerbeek, *Dent. Mater.*, 2011, **27**, 723–747.
- 5 F. Khan, M. Tanaka and S. R. Ahmad, *J. Mater. Chem. B*, 2015, **3**, 8224–8249.
- 6 J. M. Noy, F. Chen, D. T. Akhter, Z. H. Houston, N. L. Fletcher, K. J. Thurecht and M. H. Stenzel, *Biomacromolecules*, 2020, **21**, 2320–2333.
- 7 H. H. Park, K. Sun, M. Seong, M. Kang, S. Park, S. Hong, H. Jung, J. Jang, J. Kim and H. E. Jeong, *ACS Macro Lett.*, 2019, **8**, 64–69.
- 8 G. Cheng, Z. Zhang, S. Chen, J. D. Bryers and S. Jiang, *Biomaterials*, 2007, **28**, 4192–4199.
- 9 T. Furuzono, K. Ishihara, N. Nakabayashi and Y. Tamada, *Biomaterials*, 2000, **21**, 327–333.
- 10 M. Tanaka, T. Hayashi and S. Morita, *Polym. J.*, 2013, **45**, 701–710.
- 11 M. Tanaka, T. Motomura, M. Kawada, T. Anzai, Yuu Kasori, T. Shiroya, K. Shimura, M. Onishi and Akira Mochizuki, *Biomaterials*, 2000, **21**, 1471–1481.
- 12 M. J. Hajipour, S. Laurent, A. Aghaie, F. Rezaee and M. Mahmoudi, *Biomater. Sci.*, 2014, **2**, 1210–1221.
- 13 M. Tanaka, S. Morita and T. Hayashi, *Colloids Surfaces B Biointerfaces*, 2021, **198**, 111449.

- 14 T. Sonoda, S. Kobayashi, K. Herai and M. Tanaka, *Macromolecules*, 2020, **53**, 8570–8580.
- 15 K. Sato, S. Kobayashi, M. Kusakari, S. Watahiki, M. Oikawa, T. Hoshiba and M. Tanaka, *Macromol. Biosci.*, 2015, **15**, 1296–1303.
- 16 T. Hoshiba, E. Nemoto, K. Sato, H. Maruyama, C. Endo and M. Tanaka, *Biomacromolecules*, 2016, **17**, 3808–3815.
- 17 K. Nishida, T. Anada, S. Kobayashi, T. Ueda and M. Tanaka, *Acta Biomater.*, 2021, **134**, 313–324.
- 18 K. Nishida, S. Sekida, T. Anada and M. Tanaka, *ACS Biomater. Sci. Eng.*, DOI:10.1021/acsbmaterials.1c01469.
- 19 K. Nishida, S. Nishimura and M. Tanaka, *Biomacromolecules*, DOI:10.1021/acs.biomac.1c01343.
- 20 R. Pankov and K. M. Yamada, *J. Cell Sci.*, 2002, **115**, 3861–3863.
- 21 E. Grigoriou, M. Cantini, M. J. Dalby, A. Petersen and M. Salmeron-Sanchez, *Biomater. Sci.*, 2017, **5**, 1326–1333.
- 22 D. Murakami, S. Kobayashi and M. Tanaka, *ACS Biomater. Sci. Eng.*, 2016, **2**, 2122–2126.
- 23 D. Murakami, Y. Segami, T. Ueda and M. Tanaka, *J. Biomater. Sci. Polym. Ed.*, 2020, **31**, 207–218.
- 24 T. Ueda, D. Murakami and M. Tanaka, *Front. Chem.*, 2018, **6**, 1–8.
- 25 C. González-García, S. R. Sousa, D. Moratal, P. Rico and M. Salmerón-Sánchez, *Colloids Surfaces B Biointerfaces*, 2010, **77**, 181–190.
- 26 L. Baugh and V. Vogel, *J. Biomed. Mater. Res. - Part A*, 2004, **69**, 525–534.
- 27 M. Salmerón-Sánchez, P. Rico, D. Moratal, T. T. Lee, J. E. Schwarzbauer and A. J. García, *Biomaterials*, 2011, **32**, 2099–2105.
- 28 J. S. Bennett, 340–354.
- 29 A. L. Main, T. S. Harvey, M. Baron, J. Boyd and I. D. Campbell, *Cell*, 1992, **71**, 671–678.
- 30 T. Hoshiba, T. Orui, C. Endo, K. Sato, A. Yoshihiro, Y. Minagawa and M. Tanaka, *RSC Adv.*, 2016, **6**, 89103–89112.
- 31 R. Anjum, K. Nishida, H. Matsumoto, D. Murakami, S. Kobayashi, T. Anada, M. Tanaka, *Coatings*, 2021, **11**, 461
- 32 B. Sivaraman, K. P. Fears and R. A. Latour, *Langmuir*, 2009, **25**, 3050–3056.
- 33 S. Kidoaki and T. Matsuda, *Langmuir*, 1999, **15**, 7639–7646.
- 34 P. J. Molino, M. J. Higgins, P. C. Innis, R. M. I. Kapsa and G. G. Wallace, *Langmuir*, 2012, **28**, 8433–8445.
- 35 P. Roach, D. Farrar and C. C. Perry, *J. Am. Chem. Soc.*, 2006, **128**, 3939–3945.
- 36 P. Roach, D. Farrar and C. C. Perry, *J. Am. Chem. Soc.*, 2005, **127**, 8168–8173.
- 37 N. Ishida, K. Matsuo, K. Imamura and V. S. J. Craig, *Langmuir*, 2018, **34**, 3588–3596.
- 38 D. Murakami, S. Nishimura, Y. Tanaka and M. Tanaka, *Mater. Sci. Eng. C*, 2021, 112596.
- 39 L. Lv, Y. Xie, K. Li, T. Hu, X. Lu, Y. Cao and X. Zheng, *Adv. Healthc. Mater.*, 2018, **7**, 1–11.
- 40 M. Berglin, E. Pinori, A. Sellborn, M. Andersson, M. Hulander and H. Elwing, *Langmuir*, 2009, **25**, 5602–5608.
- 41 T. Ueda, D. Murakami and M. Tanaka, *J. Polym. Sci.*, 2021, **59**, 2763–2770.
- 42 I. Kiesel, M. Paulus, J. Nase, S. Tiemeyer, C. Sternemann, K. Rüster, F. J. Wirkert, K. Mende, T. Büning and M. Tolan, *Langmuir*, 2014, **30**, 2077–2083.
- 43 F. S. Ruggeri, B. Mannini, R. Schmid, M. Vendruscolo and T. P. J. Knowles, *Nat. Commun.*, 2020, **11**, 1–9.
- 44 Y. C. Yong, Y. Z. Wang and J. J. Zhong, *Curr. Opin. Biotechnol.*, 2018, **54**, 106–113.
- 45 K. Weitzel, F. Chemie, M. S. Rev, I. Introduction and C. Reference, *WHO Libr. Cat. Data*, 2011, 221–235.